

Measuring the primordial gravitational wave background in the presence of other stochastic signals

D. Poletti

International School for Advanced Studies (SISSA),
Via Bonomea 265, 34136, Trieste, Italy

Institute for Fundamental Physics of the Universe (IFPU),
Via Beirut 2, 34014 Trieste, Italy

National Institute for Nuclear Physics (INFN) Sezione di Trieste,
Padriciano, 99, 34149 Trieste, Italy

E-mail: davide.poletti@sissa.it

Abstract. Standard methodologies for the extraction of the stochastic gravitational wave background (SGWB) from auto- or cross-correlation of interferometric signals often involve the use of a filter function. The standard optimal filter maximizes the signal-to-noise ratio (SNR) between the total SGWB and the noise. We derive expressions for the optimal filter and SNR in the presence of a target SGWB plus other unwanted components. We also generalize the methodology to the case of template-free reconstruction. The formalism allows to easily perform analyses and forecasts that marginalize over foreground signals, such as the typical $\Omega_{\text{GW}} \propto f^{2/3}$ background arising from binary coalescence. We demonstrate the methodology with the LISA mission and discuss possible extensions and domains of application.

Contents

1	Introduction	1
2	The stochastic backgrounds of gravitational waves	2
3	Measuring the stochastic background	3
3.1	Standard optimal filtering	5
3.2	A new generalized filter: accounting for unwanted components in the SGWB	5
4	Template-free reconstruction	6
5	An example application: the LISA mission	8
5.1	The LISA experiment	8
5.2	The SGWB	8
5.3	Results for the A channel	9
5.4	Joint constraints from the A and E channels	11
5.5	Template-free reconstruction with the A channel	12
6	Discussion and conclusions	13
A	Derivation of the new filter	15
B	Non-linear SGWB models	16
C	A closer look to the template-free reconstruction	17

1 Introduction

Measuring the stochastic gravitational wave background (SGWB) is among the main objectives of existing and planned gravitational wave observatories. It is expected to be produced by a wide variety of astrophysical or cosmological phenomena, see [1–4] for reviews. An astrophysical SGWB certainly exists. In the recent years, we have witnessed a series of detections of gravitational waves transient signals produced by binary black holes and binary neutron stars mergers [5–11]. The signal produced by these systems, integrated over the whole history of the universe, must constitute a background of gravitational waves. Other contributions are expected to come from core-collapse supernovae, non-axisymmetric spinning neutron stars and magnetars (see, e.g., [12–15]). The background of gravitational waves produced through these mechanisms offers a window on a large number of astrophysical processes over the entire history of the universe.

The SGWB is also considered a major probe of inflation [16–19]. By postulating a period of accelerated expansion before the standard Big-Bang universe, inflation is capable of solving the horizon, flatness and monopole problems. The standard inflationary mechanism typically involves a particle beyond the Standard Model dominating the energy content of the infant universe. Its quantum fluctuations—blown up by the quasi-De Sitter expansion—naturally act as seeds of the cosmological structures we observe in the low redshift universe as well as the acoustic waves observed in the cosmic microwave background (CMB) at $z \simeq 1100$.

Quantum fluctuation of the gravitational field itself are expected to undergo a similar fate and additional GW contributions may arise from the presence of fields in addition or in place of the simple scalar-field inflaton. The resulting SGWB should be still present today at the frequencies of existing and planned GW direct detection experiments. Likewise these GW would leave an imprint in the CMB, best observable in the sought-after B-mode polarization, key target of the ultimate (or near ultimate) CMB observatories [20, 21].

Topological strings [22, 23] and superstrings [24, 25] attracted a lot of attention in this context. They also generate a SGWB resulting from the superposition of powerful bursts of GWs produced by cusps and kinks propagating on string loops. Again, this type of stochastic background can be constrained with both CMB [26] and direct detection experiments [27].

Either cosmological or astrophysical, no detection of SGWB was obtained so far. Nevertheless, the measurements of individual gravitational wave events [5–11] allowed to refine the predicted amplitude of the SGWB from compact binary coalescences [28, 29] at 25 GHz—the frequency where the aLIGO and aVIRGO observatories are most sensitive to the SGWB. Moreover, at the other end of the frequency spectrum—in the 1-100 nHz range—the common-spectrum stochastic signal detected by the NANOGrav Collaboration across an array of 45 pulsars [30] may be sourced by a SGWB, even though we have to wait for conclusive evidence of the quadrupolar correlations [31] before claiming a detection of SGWB and making inferences on its origin.

It is clear that some form of SGWB exists and, given the wide variety of possible origins, the analyses (as well as forecasts) will have to account for the possibility that multiple background sources are contributing at the same time. The problem has been already explored [32–34]. In [34], in particular, it was recognised that under some conditions the SGWB extraction and foreground rejection reduces to a linear problem. This paper effectively pushes further this consideration. We take a different perspective that we believe will make the problem (and solution) more natural and clear to the readers familiar to the popular approach to the foreground-free problem by [35, 36]. In particular, we describe their procedure in Section 3, after briefly summarizing the main quantities involved in the studies of SGWBs (Section 2). It is based on the correlation of interferometry signals employing a frequency-dependent filter, which determines the optimality of the correlation. The optimal filter is known to be essentially equal to the ratio between the strain of the SGWB and the strain-equivalent noise variance of the two signals being correlated (Section 3.1). However, if we are interested in only one of the components of the SGWB, the filter can be amended to optimally marginalize over the unwanted components—in addition to optimally coadding the contributions of the different frequencies, as done by the standard filter. We propose this new filter in Section 3.2 (see Appendix A for the demonstration) and apply it on the LISA example in Section 5. In Section 4 and Appendix C we generalize the approach to allow the reconstruction of SGWBs that are not known a priori.

2 The stochastic backgrounds of gravitational waves

We summarize here the key definitions about isotropic and unpolarized SGWB, to which we restrict ourselves in the present paper. The background of gravitational waves can be expressed as a plane wave expansion of the metric perturbation in the transverse-traceless gauge as

$$h_{ab}(t, \vec{x}) = \sum_P \int_{-\infty}^{\infty} df \int_{S^2} d^2\hat{n} h_p(f, \hat{n}) e^{i2\pi f(t - \hat{n}\cdot\vec{x}/c)} e_{ab}^P(\hat{n}) , \quad (2.1)$$

where the wave vector has been expressed in terms of its normalization and the unit vector specifying the direction of propagation, $\vec{k} \equiv 2\pi f \hat{n}/c$. We project the polarization state of the gravitational wave on the “plus” and “cross” bases, $P = +, \times$,

$$e_{ab}^+(\hat{n}) = \hat{m}_a \hat{m}_b - \hat{n}_a \hat{n}_b, \quad (2.2)$$

$$e_{ab}^\times(\hat{n}) = \hat{m}_a \hat{n}_b + \hat{n}_a \hat{m}_b, \quad (2.3)$$

where \hat{m} and \hat{n} are unit vectors orthogonal to \hat{n} and to each other. Note that the basis is normalized such that $e_{ab}^P e^{P',ab} = 2\delta^{PP'}$. In this article we assume that the observed gravitational waves belong to a SGWB that is Gaussian distributed, with zero mean and variance

$$\langle h_P^*(f, \hat{n}) h_{P'}(f', \hat{n}') \rangle = \frac{1}{8\pi} \delta^2(\hat{n}, \hat{n}') \delta_{PP'} \delta(f - f') S_h(f), \quad (2.4)$$

where the delta functions reflect the assumption that the background is isotropic, unpolarized and stationary. The spectral density function $S_h(f)$ is a real function satisfying $S_h(-f) = S_h(f)$. Eq. (2.4) also sets our convention for its normalization, which varies across the literature and in our case satisfies

$$\sum_P \int d\hat{n} \langle h_P^*(f, \hat{n}) h_{P'}(f', \hat{n}') \rangle = \delta(f - f') S_h(f). \quad (2.5)$$

The information carried by S_h is often expressed in terms of

$$\Omega_{\text{gw}}(f) \equiv \frac{1}{\rho_{\text{cr}}} \frac{d\rho_{\text{gw}}(f)}{d \ln f}, \quad (2.6)$$

where $\rho_{\text{cr}} = 3c^2 H_0^2 / 8\pi G$ is the critical density of the universe today and

$$\rho_{\text{gw}} = \frac{c^2}{32\pi G} \langle \dot{h}_{ab}(t, \vec{x}) \dot{h}^{ab}(t, \vec{x}) \rangle \quad (2.7)$$

is the energy density in gravitational waves. Given our convention, Ω_{gw} and S_h are related by

$$\Omega_{\text{gw}}(f) = \frac{4\pi^2}{3H_0^2} f^3 S_h(f) \quad (2.8)$$

3 Measuring the stochastic background

The output of a gravitational wave detector I is a time stream

$$d_I(t) = s_I(t) + n_I(t). \quad (3.1)$$

The signal s is a real function of time and is sourced by the gravitational waves hitting the detector

$$s_I(t) = \sum_{P=+,\times} \int_{-\infty}^{\infty} df \int d^2 \hat{n} F_I^P(\hat{n}, f) h_p(f, \hat{n}) e^{i2\pi f(t - \hat{n} \cdot \vec{x}_I/c)}, \quad (3.2)$$

where \vec{x} is the location of the detector and the response function $F_I^P(\hat{n}, f)$ depends on properties of the detector such as the geometry and orientation—which we assume constant in

time. The noise term n_I is also a real quantity, assumed to be stationary and Gaussian, with variance given by

$$\langle \tilde{n}_I(f) \tilde{n}_J^*(f') \rangle = \frac{1}{2} \delta(f - f') N_{IJ}(f) . \quad (3.3)$$

The 1/2 prefactor is conventional but, unlike the one of S_h , this normalization is consistent across the literature. Note that in Eq. (3.3) we have considered the possibility that I and J are different detectors with correlated noise, as in the case of the XYZ channels of the LISA mission [37].

The searches of stochastic gravitational wave backgrounds typically involve the correlation of (possibly different) detectors, I and J , both collecting signal over a time T

$$x_{IJ} \equiv \int_{-T/2}^{T/2} dt \int_{-T/2}^{T/2} dt' \left(d_I(t) d_J(t') - \frac{1}{2} N_{IJ}(|t - t'|) \right) Q_{IJ}(t, t') . \quad (3.4)$$

$N_{IJ}(|t - t'|)/2 = \langle n_I(t) n_J(t') \rangle = \int_{-\infty}^{\infty} df e^{i2\pi f(t-t')} N_{IJ}(f)/2$ sources the noise bias. The filter function Q can be arbitrarily chosen in order to maximize the signal-to-noise of the cross correlation. In Section 3.1 and 3.2, we discuss in detail the optimization of Q . For time being, we only note that because of the stationarity of both signal and noise, Q must be a function of $|t - t'|$. We assume now that $Q(|t - t'|)$ is non-negligible only for time differences much smaller than the observation time. This allows to push to infinity the extremes of one of the integrals in Eq. (3.4), and thus to get¹

$$x_{IJ} = \int_{-\infty}^{\infty} df \int_{-\infty}^{\infty} df' \delta_T(f - f') \tilde{d}_I^*(f) \tilde{d}_J(f') \tilde{Q}_{IJ}(f') - \frac{T}{2} \int_{-\infty}^{\infty} df N_{IJ}(f) \tilde{Q}_{IJ}(f) . \quad (3.5)$$

The function $\delta_T(f) = \sin(\pi f T)/\pi f$ has the following properties. It converges to the Dirac δ function as $T \rightarrow \infty$. In the same limit, δ_T^2 converges to $T\delta$. For finite T , $\delta_T(0) = T$.

The expected value and variance of x can be computed from those of $\tilde{d}_I^*(f) \tilde{d}_J(f')$, which in turn have simple expressions thanks to Eqs. (2.5), (3.2) and (3.3)—assuming that all the non-stationary, anisotropic or polarized signals have been removed or are negligible—,

$$\langle x_{IJ} \rangle = T \int_0^{\infty} df S_h(f) \mathcal{R}_{IJ}(f) \tilde{Q}_{IJ}(f) , \quad (3.6)$$

where we have defined the response function

$$\mathcal{R}_{IJ}(f) \equiv \frac{1}{4\pi} \int_{S^2} d^2 \hat{n} \sum_P F_I^{*P}(\hat{n}, f) F_J^P(\hat{n}, f) e^{-i2\pi f \hat{n} \cdot (\vec{x}_J - \vec{x}_I)/c} , \quad (3.7)$$

which depends on the properties of the detectors and their relative distance and orientation.

The variance receives a contribution from both the signal and noise, but the noise power is typically much higher than the signal. Therefore, we can ignore s in the time streams of the detectors and get

$$\langle x_{IJ}^2 \rangle - \langle x_{IJ} \rangle^2 = \frac{T}{2} \int_0^{\infty} df (N_{II}(f) N_{JJ}(f) + N_{IJ}^2(f)) |\tilde{Q}(f)|^2 , \quad (3.8)$$

The following two sections discuss how to optimize the signal-to-noise ratio.

$$\text{SNR} = \frac{\langle x_{IJ} \rangle}{\sqrt{\langle x_{IJ}^2 \rangle - \langle x_{IJ} \rangle^2}} \quad (3.9)$$

¹The tilde denotes the Fourier transform, defined as $\tilde{g}(f) \equiv \int_{-\infty}^{\infty} dt e^{-2\pi f t i} g(t)$

3.1 Standard optimal filtering

In this section we derive the standard expression of the optimal Q [35, 36], thus summarizing the approach commonly adopted in the literature and paving the road for the new filter that we propose in the next section.

We want to find the $Q(f)$ that maximises the SNR. In order to do it, it is very convenient to express Eqs. (3.6) and (3.8) in term of the following inner product of complex functions

$$\mathbf{a} \cdot \mathbf{b} = \frac{T}{2} \int_0^\infty df a^*(f) b(f) N^2(f) \quad (3.10)$$

where we have defined for convenience

$$N^2(f) \equiv N_{II}(f) N_{JJ}(f) + N_{IJ}^2(f) , \quad (3.11)$$

In contrast with the entire existing literature, we include T in the definition of the inner product. We denote with boldface the objects (lowercase for vectors and upper case for matrices) that obey to this inner product. For convenience we define the following vectors

$$\mathbf{h} \equiv \frac{2 S_h(f) \mathcal{R}_{IJ}(f)}{N^2(f)} \quad (3.12)$$

$$\mathbf{q} \equiv \tilde{Q}(f) \quad (3.13)$$

The expression for the SNR becomes

$$\text{SNR}^2 = \frac{(\mathbf{q} \cdot \mathbf{h})^2}{\mathbf{q} \cdot \mathbf{q}} , \quad (3.14)$$

which is obviously independent of the normalization of \mathbf{q} and is maximized when the vector \mathbf{q} is aligned to \mathbf{h} . The optimal filter is thus

$$\tilde{Q}(f) \propto \frac{\mathcal{R}_{IJ}(f) S_h(f)}{N^2(f)} \quad (3.15)$$

and the signal-to-noise achieved is

$$\text{SNR}^2 = 2T \int_0^\infty df \frac{|\mathcal{R}_{IJ}(f)|^2 S_h^2(f)}{N^2(f)} . \quad (3.16)$$

Other expressions in the literature do not have the factor 2. This is either because their integral ranges from $-\infty$ to ∞ or due to the fact they are considering an auto-correlation of a channel I , in which case $N^2(f) = 2N_{II}^2(f)$.

3.2 A new generalized filter: accounting for unwanted components in the SGWB

The filter presented in the previous section has one limitation: It can only optimize the detection of a single, global gravitational wave background. In particular, it can not accommodate for the presence of multiple components with unknown relative amplitudes, or with amplitudes known up to some uncertainty. We now propose a new filter capable of handling this generalized SGWB.

We study explicitly the case of a two-components SGWB

$$S_h(f) = S_p(f) + \alpha S_a(f), \quad (3.17)$$

where we want to optimize the filter $\tilde{Q}(f)$ for the measurement of a primordial SGWB $S_p(f)$, in the presence of an astrophysical contribution with known shape $S_a(f)$ and unknown amplitude α , which is the only free parameter of the model. We comment on models with non-linear free parameters in Appendix B. We allow for some external information on α to be available. We indeed assume its expected value to be $\bar{\alpha}$ and its variance σ^2 . The lack of such external information is represented by the limit $\sigma \rightarrow \infty$.

It is natural to amend the cross-correlation estimator to remove the expected contribution from astrophysical sources

$$y_{IJ} = x_{IJ} - \bar{\alpha} T \int_0^\infty df S_a(f) \mathcal{R}_{IJ}(f) Q_{IJ}(f). \quad (3.18)$$

Note that the noise bias removed in Eq. (3.5) is not any different from the removal of an astrophysical component with $\sigma = 0$.

In this more general data model, the optimal filter becomes

$$\tilde{Q}(f) \propto \frac{\mathcal{R}_{IJ}(f) S_p(f)}{N^2(f)} - \frac{\mathcal{R}_{IJ}(f) S_a(f)}{N^2(f)} \frac{2T \int_0^\infty df' |\mathcal{R}_{IJ}(f')|^2 S_a(f') S_p(f') N^{-2}(f')}{\sigma^{-2} + 2T \int_0^\infty df' |\mathcal{R}_{IJ}(f')|^2 S_a(f') S_a(f') N^{-2}(f')}. \quad (3.19)$$

and the corresponding SNR is

$$\text{SNR}^2 = 2T \int_0^\infty df \frac{|\mathcal{R}_{IJ}(f)|^2 S_p^2(f)}{N^2(f)} - \frac{[2T \int_0^\infty df |\mathcal{R}_{IJ}(f)|^2 S_a(f) S_p(f) N^{-2}(f)]^2}{\sigma^{-2} + 2T \int_0^\infty df |\mathcal{R}_{IJ}(f)|^2 S_a^2(f) N^{-2}(f)}. \quad (3.20)$$

We report the derivation in Appendix A, where we consider the even more general case of an arbitrary number of contributions to $S_h(f)$.

In both Eq. (3.19) and (3.20), the first term corresponds to the standard filter and SNR, reported in Eqs. (3.15) and (3.16). The second term is the correction that accounts for the presence of the astrophysical component in the SGWB. Note that in Eq. (3.20) this term is always negative, reflecting the intuition that the presence of astrophysical sources can only degrade the SNR.

Looking at the numerator more closely, the integral (and thus the SNR degradation) is maximum when the primordial and astrophysical components have the same frequency dependence. When this happens the SNR becomes

$$\text{SNR}^2 = \frac{2T \int_0^\infty df |\mathcal{R}_{IJ}(f)|^2 S_p^2(f) N^{-2}(f)}{1 + \sigma^2 2T \int_0^\infty df |\mathcal{R}_{IJ}(f)|^2 S_a^2(f) N^{-2}(f)} \quad \text{for} \quad S_a(f) \propto S_p(f), \quad (3.21)$$

which is zero for $\sigma \rightarrow \infty$: When the primordial and astrophysical SGWB have the same frequency dependence, nothing can be said on the primordial component if no external information on the astrophysical one is available.

Focusing now on the denominator of the second term in Eq. (3.20), it represents the total information about the amplitude of the astrophysical SGWB. It is clearly separated into the external and the internal contribution, with the latter always overtaking the former for sufficiently long observational times.

4 Template-free reconstruction

Building on the approach illustrated in the previous section, we now extend the discussion to the reconstruction of the primordial SGWB without assuming a template for it. More details

are provided in Appendix C, together with the general expression for an arbitrary number of foreground components.

We consider the following quantity,

$$z_{IJ}(f) \equiv \frac{2}{T\mathcal{R}_{IJ}(f)} \int_0^\infty df' (d_I^*(f)d_J(f') + d_I(f)d_J^*(f')) \delta_T(f-f') - \frac{N_{IJ}(f)}{\mathcal{R}_{IJ}(f)} - \bar{\alpha}S_a(f). \quad (4.1)$$

It is essentially an elaboration on Eq. (3.5), without the integration over f . The two terms inside the integral (instead of one) have the only effect of folding the integral, which ranges over positive values of f' . $z_{IJ}(f)$ can already be considered a template-free reconstruction, as the expected value is $\langle z_{IJ}(f) \rangle = S_p(f)$: All the terms outside of the integral just remove additive and multiplicative biases. Its variance is

$$V(f, f') = \frac{N^2(f)\delta(f-f')}{2T|\mathcal{R}_{IJ}(f)|^2} + \sigma^2 S_a(f)S_a(f'). \quad (4.2)$$

and its inverse is equal to

$$F(f, f') = \frac{2T|\mathcal{R}_{IJ}(f)|^2}{N^2(f)}\delta(f-f') - \frac{[2T|\mathcal{R}_{IJ}(f)|^2S_a(f)N^{-2}(f)] [2T|\mathcal{R}_{IJ}(f')|^2S_a(f')N^{-2}(f')]}{\sigma^{-2} + 2T \int_0^\infty df'' |\mathcal{R}_{IJ}(f'')|^2 S_a^2(f'') N^{-2}(f'')}. \quad (4.3)$$

In the Gaussian approximation F coincides with the Fisher matrix, the information available for any SGWB model for the given experimental configuration. In any case, it is related to the SNR on a specific model in Eq. (3.20) by

$$\text{SNR}^2 = \int_0^\infty df \int_0^\infty df' F(f, f') S_p(f') S_p(f). \quad (4.4)$$

z_{IJ} is typically very noisy and it should be used as an intermediate step towards its projection onto a subspace defined by a set of model spectra. These modes can be motivated by the theory (e.g., SGWB spectra from a class of physically motivated models), by a target property of the reconstructed spectrum (e.g., polynomials of varying nature or some type of smooth functions to avoid sharp features) or by the constraints that the experiment can provide over them. The principal component analysis (PCA) is part of this last category and its usage in this context was already proposed by [34]. Our explicit expression for the Fisher information allows to better understand (and exploit) its structure, and to properly compute its eigenvectors and eigenvalues (see Appendix C). PCA consists in selecting the k largest eigenvalues of F , λ_i , and projecting z_{IJ} onto the corresponding eigenvectors, $v_i(f)$, which represent the uncorrelated modes in our measurement². The estimated spectrum is

$$\hat{S}_p(f) = \sum_{i=1}^k v_i(f) \int_0^\infty df' v_i(f') z_{IJ}(f'), \quad (4.5)$$

and has a total SNR equal to

$$\text{SNR}^2 = \sum_{i=1}^k \lambda_i \left[\int_0^\infty df' v(f') z_{IJ}(f') \right]^2. \quad (4.6)$$

² λ_i and $v_i(f)$ can be equivalently computed either from the Fisher or the covariance matrix. The covariance has an easier expression while the Fisher matrix handles more naturally $\sigma \rightarrow \infty$.

These expressions are particularly simple compared to the corresponding expressions for any other basis of models on which to project z_{IJ} (compare with Eqs. (C.5-C.6)). Moreover, F is a diagonal matrix plus a (very-)low-rank correction, which makes the computation of the eigenvectors cheap even for a large number of frequencies. However, we believe that the PCA is not very interesting in this context. The reason is that this structure of F also makes the eigenvectors very similar to delta functions, which in turn makes the PCA only marginally different from the selection of a frequency interval in the trough of the noise curve. Projecting on a different basis of models is reasonably simple anyway: It is essentially a generalized least squared estimation (see Appendix C for more details and Section 5.4 for an example).

5 An example application: the LISA mission

In this section we show an example of how the formalism of the previous section can be applied. We forecast the performance of the LISA mission attempting to detect a specific model of primordial SGWB in the presence of an astrophysical signal.

5.1 The LISA experiment

The Laser Interferometer Space Antenna (LISA) [38] is the most advanced project for a gravitational wave antenna in space. It is an ESA L-class mission with a NASA partnership and it is planned for launch in the early/mid 2030s. The experiment consists in three spacecraft, 2.5 million km apart, in a triangular configuration. Laser links between the spacecrafts will provide three interferometry measurements which will monitor the relative distance between the test masses in the spacecrafts, allowing to probe the space-time distortion due to incoming gravitational waves. Each of the three pair of arms provide an interferometry measurement—a time series as the one in Eq. (3.1). These are the so-called XYZ channels. These signals are correlated but, thanks to the symmetry of the configuration, it is easy and natural to extract their eigenmodes, dubbed AET channels, given by

$$d_A = (d_X - 2d_Y + d_Z)/\sqrt{6} \quad (5.1)$$

$$d_E = (d_X - d_Z)/\sqrt{2} \quad (5.2)$$

$$d_T = (d_X + d_Y + d_Z)/\sqrt{3}. \quad (5.3)$$

While A and E have identical noise properties and response function, those of the T channel are very different and make this latter channel much less sensitive than the former ones (see Figure 1). We also convert the A/E noise PSD to energy density Ω_{GW} with Eq. (2.8) and display it in Figure 3. The calculation of the noise curves as well as the response functions³ follows [39] and make the same simplifying assumptions. For example, we assume that there is no gap in the data, the noise is perfectly stationary and we ignore the time dependence of the response function due to the orbital motion of the spacecrafts. We refer the reader to this article for more details.

5.2 The SGWB

We consider two types of backgrounds of astrophysical origin. The first one, is sourced by the incoherent superposition of the emission of compact binaries that are not individually resolved by the experiment—mostly stellar-origin black holes and neutron star binaries

³For the response functions we use the tabulated numerical values that the authors made available at <https://doi.org/10.5281/zenodo.3341817>

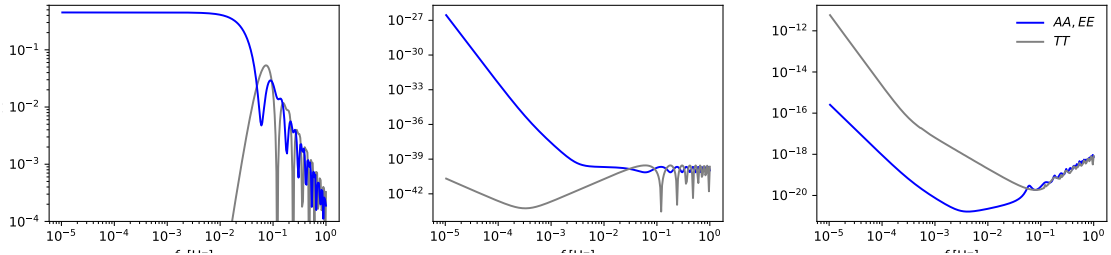


Figure 1. The main properties of the A , E and T channels of LISA, the experimental configuration considered in the demonstration in Section 5. *Left:* Response function. *Center:* Noise power spectral density. *Right:* Characteristic strain sensitivity.

(BBH+BNS). This signal is well approximated by a power law [4]

$$\Omega_{\text{GW}}(f)h^2 = \Omega_* \left(\frac{f}{f_*} \right)^{2/3}, \quad (\text{BBH} + \text{BNS}) \quad (5.4)$$

The reference value we use is $\Omega_* = 8.9 \times 10^{-10}$ at $f_* = 25$ Hz [40] but we consider it an unknown parameter to marginalize over. We assume that a prior on it is available, it is centered around the reference value and has a standard deviation given by $\sigma_{\text{BBH+BNS}}$

The second type of astrophysical background that we consider is sourced by unresolved galactic binaries (UGB). We model its contribution with [41, 42]

$$S(f) = Af^{-7/3} e^{-f^\alpha + \beta f \sin \kappa f} [1 + \tanh(\gamma(f_k - f))] \text{ Hz}^{-1}, \quad (\text{UGB}) \quad (5.5)$$

which we convert to Ω_{GW} with Eq. (2.8). We fix the free parameters to the following values, which refer to a 4 year-long LISA mission, $\alpha = 0.138$, $\beta = -221$, $\kappa = 521$, $\gamma = 1680$ and $f_k = 0.00113$ [42]. Our reference value for the normalization factor A is 9×10^{-45} but, also here, we treat it as a free parameter with some prior constraint centered at the reference value and a standard deviation given by σ_{UGB} .

Finally the primordial SGWB that we consider is the AX1 model of [43]—which is produced by a spectator axion-SU(2) model. The origin and properties of such a background are, however, irrelevant for our analysis. We choose this model only for illustration purposes and are motivated mostly by its amplitude, which makes such a background within reach for the instrumental configuration of our choice.

We display the three components of the measured background in Figure 3. Their different frequency dependence is the main feature that our methodology exploits, while their amplitudes constitute the free parameters of the model.

5.3 Results for the A channel

We now apply the formalism of Section 3.2 to the LISA A channel and study the new filter and SNR. The results for the E channel would be of course identical, while the T channel is noise dominated and we do not report results about it.

We consider values of σ_{UGB} ranging from 10^{-4} and 10^{-2} and values of $\sigma_{\text{BBH+BNS}}$ ranging from 10^{-3} and 10^{-1} . As we will see, the lower values correspond to the case where the external information completely constrains the astrophysical component, the higher value is equivalent to the case where no external information is available. We stress that the range of values for

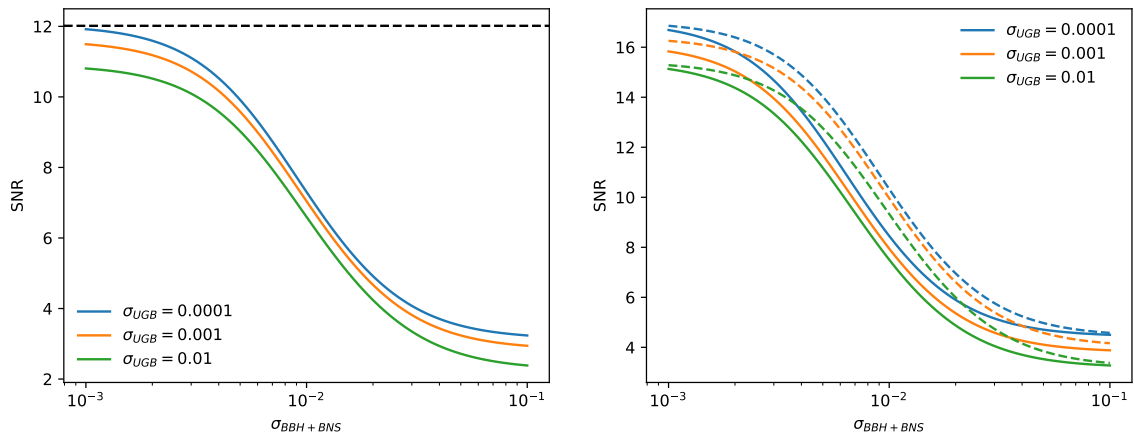


Figure 2. *Left:* Signal-to-noise ratio from either the A or E channel, for varying values of σ_{UGB} and $\sigma_{\text{BBH+BNS}}$, computed with Eq. (3.20)—actually Eq. (A.11), because we are dealing with multiple astrophysical sources. For reference, the black dashed line reports the SNR obtained with the standard formula Eq. (3.16) ignoring the astrophysical components. *Right:* Signal-to-noise ratio from the A and E channels combined. The dashed line reports what one would get with a naive co-addition of the SNR of the individual channels (i.e. multiplying them by $\sqrt{2}$).

σ_{UGB} and $\sigma_{\text{BBH+BNS}}$ is chosen only to best illustrate the phenomenological properties of our formalism and does not stem from an instrumental or theoretical forecast. Also the inclusion of this level of UGB is not fully realistic, as this signal can be removed exploiting its time dependence owing to the motion of the spacecrafts [44].

The filter We start by focusing on the effect that the astrophysical components have on the filter Eq. (3.19)—and Eq. (A.10). The three panels of Figure 3 refer to three different amounts of external information on the extra-galactic binaries, while the three colors represent different priors on the galactic binaries. The dashed line reports the standard filter, which only performs inverse noise co-addition: it is always positive and significantly larger than zero only between 0.4 mHz and 10 mHz. The blue line in the top panel represents the case in which the amplitude of both the astrophysical backgrounds is very constrained by external information. This case reduces to the standard filter, as mentioned in Section 3.2. When σ_{UGB} increases to 0.001 (orange line) the filter give less weight to the frequencies around 1 mHz in order to reduce the response to the UGB signal—which peaks at these frequencies, see the figure on the left. When σ_{UGB} reaches 0.01 (green line) the amplitude of the signal from galactic binaries is so uncertain that the filter is required to have zero response to the UGB signal shape. This can only be achieved with a negative region in the filter: The trough around 1 mHz that the green lines have in all the panels.

A completely analogous discussion can be done about the BBH and BNS signal, whose amplitude with respect to the other components increases with frequency—even though it is shadowed by the noise above 10 mHz. This is the reason why the filter with $\sigma_{\text{BBH+BNS}} = 0.01$ (middle panel) gives slightly less weight compared to the case with $\sigma_{\text{BBH+BNS}} = 0.001$ (top panel) and the same region becomes negative for $\sigma_{\text{BBH+BNS}} = 0.1$.

As a final remark, we note that the peak of the filter increases when the amount of external information is reduced. This is a consequences of the fact that when displaying these

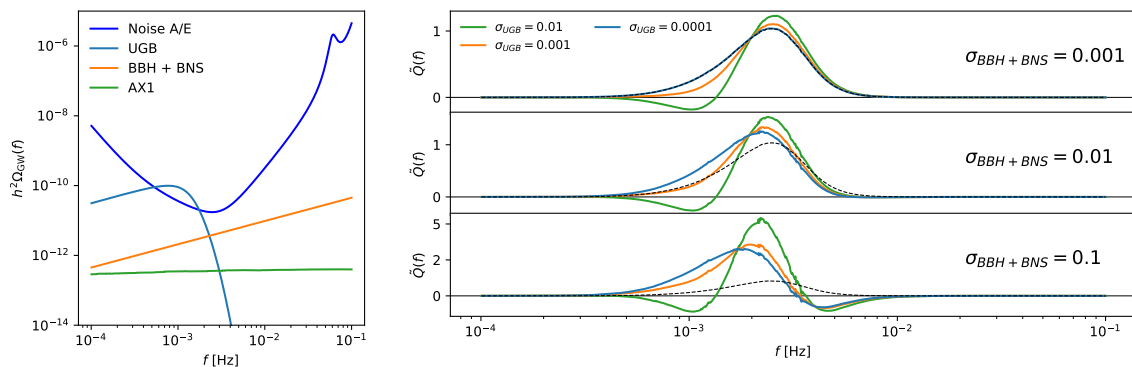


Figure 3. *Left:* Components of the SGWB considered in application of the methodology. The noise equivalent Ω_{GW} for the A (or E) channel is also reported. *Right:* Shape of the filter functions for different values of σ_{UGB} (color) and $\sigma_{\text{BBH+BNS}}$ (subplots). For comparison, the standard filter is the dashed back line.

filters we impose that they have the same response to the target primordial signal⁴. Therefore, the decreased (or negative) weight in the frequencies dominated by the astrophysical emission is compensated with an increased weight around the minimum of the astrophysical emission.

The SNR We now study the SNR achieved for the same configuration and external information about the astrophysical components. The result is reported in Figure 2, where we also draw the standard SNR (black dashed line) computed with Eq. (3.16) ignoring the presence of astrophysical sources. First note that this value coincides with the SNR obtained for $\sigma_{\text{BBH+BNS}} = 0.0001$ and $\sigma_{\text{UGB}} = 0.001$, when the amplitude of the astrophysical signals is completely constrained by the external prior and therefore there is no information loss while marginalizing over them (blue line, left end). Looking at the other extreme, if the amplitude of the astrophysical components is completely unconstrained ($\sigma_{\text{BBH+BNS}} = 0.01$ and $\sigma_{\text{UGB}} = 0.1$, green line, right end), the rejection of their signal severely degrades the SNR from 12 to 2.4, which corresponds to a 96% information loss. This should be largely ascribed to the BBH+BNS, as even with $\sigma_{\text{BBH+BNS}} = 0.0001$ (blue line) the information loss is still 93%. The reason is simple: The frequency dependence of the primordial signal is much more orthogonal to the one of the UGB than the one of the BBH+BNS.

5.4 Joint constraints from the A end E channels

The only purpose of this section is to stress a supposedly obvious fact that is however easy to forget: Using the same prior information across multiple measurements correlates the constraints they produces, and they can not be combined as if they were independent.

One of the most attractive properties of working with the AET channels compared to the XYZ channels is the fact that the cross-channel power is zero and they are statistically equivalent to independent experiments, at least in our idealised treatment. Moreover, the A and E channels have the same noise level and, therefore, combining them effectively doubles the statistical information provided by the individual channel and, in the standard case Eq. (3.16), $\text{SNR}_{A+E}^2 = \text{SNR}_A^2 + \text{SNR}_A^2 = 2\text{SNR}_A^2$.

⁴We remind that the normalization of the filter is arbitrary and does not affect its optimality

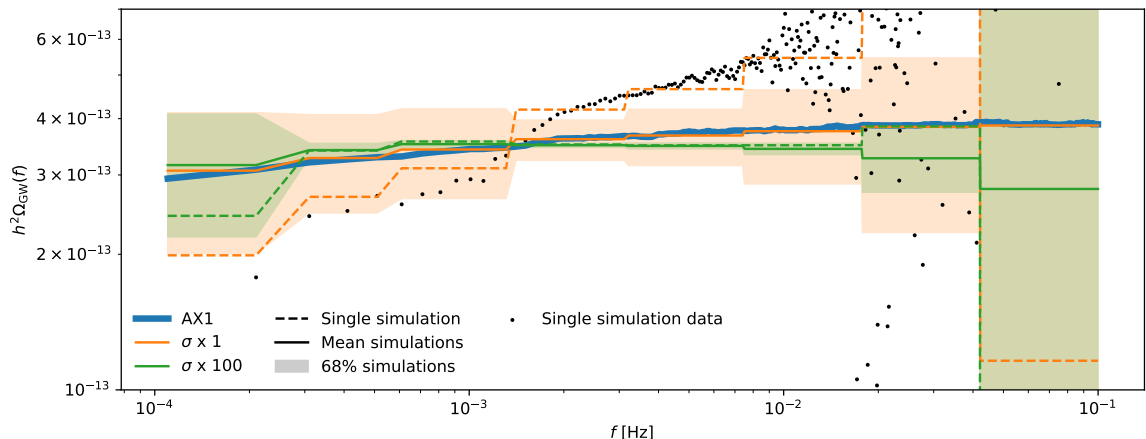


Figure 4. Template-free reconstruction. The thick blue line is the target signal. The orange represents the estimators that assume the same σ_{UGB} and $\sigma_{\text{BBH+BNS}}$ used for simulating the data, while the green assumes one hundred times larger values. The solid lines are the median of 10^4 simulated reconstructions and the shaded areas covers from the 16th to the 84th percentile. As an example, we also show the data (dots) and the reconstruction (dashed lines) for a single simulation.

The formalism in Section 3.2, however, can accommodate external information, which may play a significant role in SNR_A and SNR_E computed with Eq. (3.20). When this happens the two SNRs are correlated and can not be added in quadrature. Instead of accounting for the correlation in their coaddition, it is easier to properly compute the joint SNR. It can be shown easily that the optimal combination of the two channels boils down to the average of the two auto-correlations, which has the same expected value and half the variance the individual channels and is therefore equivalent to the A (or E) channel with a N divided by $\sqrt{2}$. SNR_{A+E}^2 can be computed with the Eq (3.20) applied to A (or E) but multiplying every integral by 2. Multiplying SNR_A^2 by two altogether, doubles the external information σ^{-2} —which, on the contrary, stays constant in SNR_{A+E}^2 .

In the right panel of Figure 2 we compare SNR_{A+E} with $\sqrt{2}\text{SNR}_A$. The two coincide whenever the the σ s are either very low or very high (the endpoints of the blue and green lines). When a σ is very low, the correction term in Eq. (3.20) is negligible in both cases, while when the σ is very high the correction term is not affected by its exact value.

Summarizing, the naive co-addition of the SNRs from independent measurements is significantly incorrect when the external information plays a significant but not overwhelming role. Note that this example of combination of the A and E channel completely analogous to the combination of separate frequency bins. Naively co-adding the SNR from arbitrarily small bins produces a total SNR arbitrary close to the standard SNR with no contaminants—which is of course unphysical (and wrong).

5.5 Template-free reconstruction with the A channel

Without assuming prior knowledge on the primordial SGWB, we perform its reconstruction from simulated data of the A channel following the prescription of Section 4 (and Appendix C). We simulate z_{AA} at linearly spaced frequencies, emulating what we would get if we were to compute it from the FFT of d_A . The signal in z_{AA} is the same primordial SGWB of the previous sections. On the top of it we add Gaussian noise generated according to the

covariance matrix Eq. (4.2) assuming $\sigma_{\text{UGB}} = 0.001$ and $\sigma_{\text{BBH+BNS}} = 0.01$. We create and analyze independently 10^4 realizations. The reconstruction is done using 8 top-hat functions with equal logarithmic width, covering the range from 0.1 mHz to 0.1 Hz. More sophisticated sets of functions are possible, of course, but this simple choice already allows to show some of the main features of our approach. The variance assumed by the template-free estimator is either the same of the simulated data, or one that assumes one hundred times larger σ_{UGB} and $\sigma_{\text{BBH+BNS}}$. This latter case essentially coincides with the absence of external information and, therefore, its inverse-variance down-weights (or filters) more aggressively the signals with the frequency dependence of the astrophysical components.

The results of the analysis are shown in Figure 4, which shows all the quantities (z_{AA} included) in terms of energy density spectrum Ω_{GW} . Focusing on the single simulation represented by the dots, it clearly shows an over-subtraction of the galactic signal and an under-subtraction of the extragalactic astrophysical signal. Our estimator differs from a simple binning because it not only does an inverse-noise-weighted average inside the bins, but also down-weights the spectral shapes that match the ones of the astrophysical signals—the larger σ , the stronger the down-weighting. The reconstructions (dashed lines) are indeed closer to the target signal than the original data. In particular, the estimator that assumes larger σ (green) filters out the spectral shapes of astrophysical origin and, therefore, it seems to mitigate better the under- and over-subtraction of the astrophysical signals. However, when many simulations are averaged (solid lines), filtering translates into a bias because the same modes are suppressed from the target signal. Instead, when the estimator uses the correct values of σ the mean reconstruction is unbiased, even though in the single simulation the astrophysical residuals do not seem to be removed as effectively—which is also reflected in the larger scatter of the simulations (orange boxes, compared to the green boxes).

As a last remark, we want to stress that inferring uncertainties from the scatter of individual frequency bins across simulations (the shaded areas in Figure 4) can be highly misleading: They represent only the diagonal of the covariance matrix, while the bins are highly correlated. Once the full covariance is taken into account (see Appendix C) one realises that the estimator that uses the correct values of σ is not only unbiased even on the single simulation but also it is truly minimum variance. The scatter in the simulations is dominated by modes that have the same frequency dependence of the astrophysical signals because these modes are highly uncertain. When they are completely filtered out not only the scatter but also the signal in those modes is removed and therefore their relative uncertainty is infinity.

6 Discussion and conclusions

The existence of some form of SGWB is well motivated both from the theory and the direct GW observations of the past years. The standard detection techniques have focused on distinguishing a template SGWB signal from the noise in the auto- or cross-correlation of interferometric signals. From the data analysis point of view, there is freedom on the filter function involved in the correlation and the optimal choice is equal to the template signal divided by the noise power variance—both diagonal in the frequency-domain.

We extend this approach to the case in which other sources are present in addition to the target SGWB. We derive the filter that optimally balances between the inverse-noise weighting done by the standard filter and the marginalization over the unwanted components, taking into account possible external priors. Both the filter and the corresponding SNR are almost as simple as the the standard ones—and reduce to them either if the amount of

external information is very large, or if the spectral shape of the unwanted components is very different from the target SGWB. In particular the optimal filter and SNR have closed-forms and all the terms are easy to compute and interpret. It is extremely simple, for example, to forecast the sensitivity of an experimental configuration to a primordial SGWB produced by an exotic inflationary model while, at the same time, marginalizing over a background $\Omega_{\text{GW}} \propto f^{2/3}$ produced by unresolved binary black holes and neutron stars [see 43]. We apply the formalism to the LISA mission and show that neglecting the marginalization over the astrophysical signals—as done by the standard estimator—can grossly overestimate the SNR. We remind that in the text we have used the terms “primordial” or “astrophysical SGWB” only for illustration purposes. The approach is perfectly applicable to contexts where the target signal has astrophysical origin or where both the target and unwanted component(s) are primordial.

Our methodology is derived and applied in the context of isotropic, unpolarized background signals, but it can be easily generalized to polarized and anisotropic signals. The only important caveat is that it is based on the assumption (standard in the literature) that the variance in the auto- or cross-correlation is dominated by the noise at all frequencies. This assumption is key in obtaining nice and simple closed-form for the optimal filter and SNR, but may be too stringent in very high SNR settings.

Compared to techniques that blindly attempt to reconstruct the SGWB, the new filter we have illustrated does require a template of the target signal. However, the filter can be relevant also to procedures that perform a more flexible SGWB reconstruction. Take for example [33], the authors perform a template-free reconstruction of a primordial SGWB while marginalizing over a set of templates with uncertain amplitude (representing the same astrophysical components we considered in Section 5). Their MCMC samples both the parameters of their non-linear primordial SGWB model and the amplitude of the astrophysical templates. If the interest lies in the former and the latter are only marginalized over, this marginalisation can be done analytically during the MCMC using the filter in Eq. (3.19) (or analogous expressions) with a signal defined by the current value of the target signal parameters in the MCMC chain. This allows to achieve the same result with reduced computational cost, as the parameters related to the astrophysical background are not explored by the Markov chain.

Moreover, we have shown how our methodology is applicable also to a template-free reconstruction of the SGWB. Provided a basis for the admissible models, the method projects the data onto the space spanned by these models, balancing noise-weighting and foreground removal. In our example we consider simple top-hat functions, but any choice is admitted—such as polynomials, harmonic functions, or a basis of the possible SGWB produced by a class of inflationary models. Albeit much richer than a single template, this type of procedure allows only linear models, but this class of parametrizations may turn out to be sufficiently flexible for many applications and fit the (simulated) data with an accuracy comparable to a more involved non-linear fit.

Acknowledgments

The author is thankful to Paolo Campeti, Eiichiro Komatsu and Carlo Baccigalupi for useful comments and discussions. The author acknowledges support from the ASI-COSMOS network (www.cosmosnet.it) and the INDARK INFN Initiative (web.infn.it/CSN4/IS/Linea5/InDark).

A Derivation of the new filter

We assume the presence of a primordial SGWB and a set of astrophysical backgrounds, due to different populations of unresolved sources,

$$S_h(f) = S_p(f) + \sum_i \alpha_i S_{a_i}(f). \quad (\text{A.1})$$

We optimize the filter for the primordial SGWB but make no use of its properties in the derivation. Likewise, the astrophysical origin of the unwanted components plays no role. The only relevant assumption for what follows is the fact that all the contributions have known frequency dependence and possibly unknown amplitude.⁵ For example, all the models that predict an $f^{-3/2}$ dependence can be accommodated (or approximated) in this formalism.

In the notation introduced in Section 3.1, the signal can be written as

$$\mathbf{h} = \mathbf{p} + \mathbf{A}\boldsymbol{\alpha}, \quad (\text{A.2})$$

where \mathbf{p} is defined similarly to Eq. (3.12). The same is done for the astrophysical sources, which are further collected in the columns of \mathbf{A} . Their amplitudes are free parameters and are collected in a vector $\boldsymbol{\alpha}$, with expected value $\bar{\boldsymbol{\alpha}}$ and covariance $\boldsymbol{\Sigma}$.

We are interested in optimizing the filter for the detection of \mathbf{p} . The cross-correlation can be corrected for the contribution of the astrophysical SGWB,

$$y_{IJ} = x_{IJ} - \mathbf{q} \cdot \mathbf{A}\bar{\boldsymbol{\alpha}}, \quad (\text{A.3})$$

so that its expected value depends only on the primordial SGWB,

$$\langle y_{IJ} \rangle = \mathbf{q} \cdot \mathbf{p}. \quad (\text{A.4})$$

The variance is

$$\langle y_{IJ}^2 \rangle - \langle y_{IJ} \rangle^2 = \mathbf{q}^t \mathbf{q} + \mathbf{q}^t \mathbf{A} \boldsymbol{\Sigma} \mathbf{A}^t \mathbf{q}, \quad (\text{A.5})$$

where $\mathbf{a}^t \mathbf{b} \equiv \mathbf{a} \cdot \mathbf{b}$. The new expression for the SNR is therefore

$$\text{SNR}^2 = \frac{(\mathbf{q}^t \mathbf{p})^2}{\mathbf{q}^t \mathbf{q} + \mathbf{q}^t \mathbf{A} \boldsymbol{\Sigma} \mathbf{A}^t \mathbf{q}}. \quad (\text{A.6})$$

Also in this case, the SNR is independent of the normalization of \mathbf{q} . We choose it such that

$$\mathbf{q}^t \mathbf{p} = \gamma, \quad (\text{A.7})$$

where γ is an arbitrary constant. We now minimize the denominator of Eq. (3.20) under the condition in Eq. (A.7), which can be readily done using Lagrange multipliers. The gradient of the Lagrangian is

$$\nabla_{\mathbf{q}} \mathcal{L}(\mathbf{q}, \lambda) = 2(\mathbf{1} + \mathbf{A} \boldsymbol{\Sigma} \mathbf{A}^t) \mathbf{q} + \lambda \mathbf{p}. \quad (\text{A.8})$$

Since the matrix in parenthesis is positive-defined, there is only the following stationary point and this point is a minimum

$$\mathbf{q} \propto (\mathbf{1} + \mathbf{A} \boldsymbol{\Sigma} \mathbf{A}^t)^{-1} \mathbf{p}. \quad (\text{A.9})$$

⁵If useful, a free parameter can be introduced also in front of the primordial contribution. Nothing would change in the expression of the optimal filter and its derivation. The only difference would be the multiplication of the SNR by the expected value of such additional parameter.

This expression is practically inconvenient because it involves the inversion of a large and dense matrix. Therefore, we use the Woodbury identity to re-express Eq. (A.9) as

$$\mathbf{q} \propto \mathbf{p} - \mathbf{A} (\Sigma^{-1} + \mathbf{A}^t \mathbf{A})^{-1} \mathbf{A}^t \mathbf{p}, \quad (\text{A.10})$$

which is the final form of our filter. The corresponding signal-to-noise ratio is

$$\text{SNR}^2 = \mathbf{p}^t \mathbf{p} - \mathbf{p}^t \mathbf{A} (\Sigma^{-1} + \mathbf{A}^t \mathbf{A})^{-1} \mathbf{A}^t \mathbf{p}. \quad (\text{A.11})$$

For the case of one single astrophysical component, we report the explicit expression of this filter and SNR in Eqs. (3.19) and (3.20).

B Non-linear SGWB models

Many models of both cosmological and astrophysical SGWB contain non-linear parameters. Therefore, we generalize our model as follows

$$S_h(f) = S_p(f) + \sum_i \alpha_i S_{a_i}(f, \beta_i). \quad (\text{B.1})$$

where β_i is a non-linear parameter⁶ in the model of the i -th astrophysical component. By Taylor expanding the data model to first order

$$S_h(f) \simeq S_p(f) + \sum_i \alpha_i S_{a_i}(f, \bar{\beta}_i) + \sum_i \bar{\alpha}_i \frac{\partial S_{a_i}}{\partial \beta_i}(f, \bar{\beta}_i) (\beta_i - \bar{\beta}_i). \quad (\text{B.2})$$

it becomes linear in the free parameters and therefore compatible with the assumptions made in the Appendix A: \mathbf{A} acquires extra columns given by all the $\bar{\alpha}_i \frac{\partial S_{a_i}}{\partial \beta_i}(f, \bar{\beta}_i)$, and $\boldsymbol{\alpha}$ acquires extra rows given by all the $\beta_i - \bar{\beta}_i$ coefficients. Of course, Σ acquires the same number of extra rows and columns, that can be used to accommodate external information about the non-linear parameters as well as their correlation with the linear ones. Note that, if they are infinity (i.e. no external information is available on the non-linear parameters), the $\bar{\alpha}_i$ factor multiplying the i -th new column of \mathbf{A} is irrelevant: Only the frequency dependence of the new column matters, not its normalization.

This natural extension of the formalism to non-linear parameters should, however, be used with care when analyzing data (or simulations). First, one should consider if the model is overly complex for the experimental configuration being analyzed. If the uncertainty on the linear parameters α_i is already very large, there is no point in refining the model of the i -th foreground. Second, even if the constraints on those parameters are good, those on the non-linear parameters might be loose. As a result, $\alpha_i S_{a_i}(f, \bar{\beta}_i) + \bar{\alpha}_i \frac{\partial S_{a_i}}{\partial \beta_i}(f, \bar{\beta}_i) (\beta_i - \bar{\beta}_i)$ for the best fit α_i and β_i may be quite far from what one would get from the fully non-linear fit of $\alpha_i S_{a_i}(f, \beta_i)$ —meaning that the linear Taylor expansion Eq. (B.2) is insufficient to describe the behaviour of the i -th astrophysical component in the range of plausible noise realizations. This occurrence may not be easy to know in advance, it could even depend on the specific noise realization. This may or may not be a problem for the constraints on the primordial component of the SGWB, depending on how degenerate $S_p(f)$ is with the difference between the linearized and fully non-linear fit. The degeneracy is typically unknown from the onset

⁶It can also be a vector of parameters, the generalization is straightforward.

and its evaluation would require to compute the non-linear fit, which would make the linear approximation of limited interest. Third, also the high signal-to-noise has a caveat: It still requires to guess $\bar{\beta}_i$. If $\frac{\partial S_{a_i}}{\partial \beta_i}$ varies noticeably between $\bar{\beta}_i$ and the true value of β_i , the linearized and non-linear best-fit could be significantly different and bias the constraints on the primordial SGWB.

On the other hand, the applicability range of the linearized data model is much wider in the realm of forecasting. The biases related to the noise realization and the imperfect choice of the reference $\bar{\beta}_i$ are indeed under control. Moreover, if the quantity of interest is only the SNR, the value obtained with the linearized data model coincides with the Fisher estimate of the constraints from the non-linear fit.

C A closer look to the template-free reconstruction

We start from the estimator in Eq. (4.1), amended to account for an arbitrary number of astrophysical components

$$z_{IJ}(f) \equiv \frac{2}{T\mathcal{R}_{IJ}(f)} \int_0^\infty df' (d_I^*(f)d_J(f') + d_I(f)d_J^*(f')) \delta_T(f - f') - \frac{N_{IJ}(f)}{\mathcal{R}_{IJ}(f)} - \sum_i \bar{\alpha}_i S_{a_i}(f). \quad (\text{C.1})$$

Its covariance is equal to⁷

$$V(f, f') = \frac{N^2(f)\delta(f - f')}{2T|\mathcal{R}_{IJ}(f)|^2} + \sum_i \sigma_i^2 S_{a_i}(f)S_{a_i}(f'). \quad (\text{C.2})$$

Since $\langle z_{IJ}(f) \rangle = S_p(f)$, V is the frequency-frequency covariance for single-sided primordial signals. The first term is the instrumental noise, while the second is the variance due to the fact that the normalization of the astrophysical component a_i is known up to a standard deviation σ_i .

From now on we assume that $z_{IJ}(f)$ is Gaussian-distributed. This is an approximation that may be oversimplistic at the full sampling rate of the experiments, but it becomes realistic if $z_{IJ}(f)$ represents an average over several independent periods or the mean of many neighbouring frequencies. In this approximation the Fisher information matrix is the inverse of the variance. To obtain readable expressions we define $\mathbf{N} \equiv N^2(f)\delta(f - f')/2T|\mathcal{R}_{IJ}(f)|^2$ and $\Sigma \equiv \text{diag}(\sigma_i)$ and collect all the astrophysical signals S_{a_i} in the columns of \mathbf{A} . Note that the operator \mathbf{A} is not exactly the same of Appendix A: The basis of the frequency domain is different. We will also use a different (and more standard) inner product: $\mathbf{a} \cdot \mathbf{b} \equiv \int_0^\infty df a(f)b(f)$. In this notation

$$V(f, f') = \mathbf{N} + \mathbf{A}\Sigma\mathbf{A}^t \quad (\text{C.3})$$

and its inverse can be obtained using the Woodbury identity

$$F(f, f') = \mathbf{N}^{-1} - \mathbf{N}^{-1}\mathbf{A}(\Sigma^{-1} + \mathbf{A}^t\mathbf{N}^{-1}\mathbf{A})^{-1}\mathbf{A}^t\mathbf{N}^{-1}. \quad (\text{C.4})$$

⁷It might be useful to remember that

$$\begin{aligned} \langle n_I^*(f)n_J(k)n_I(f')n_J^*(k') \rangle - \langle n_I^*(f)n_J(k) \rangle \langle n_I(f')n_J^*(k') \rangle &= \frac{1}{4}[\delta(f - f')\delta(k - k')N_{II}(f)N_{JJ}(k) + \\ &+ \delta(f + k')\delta(f' + k)N_{IJ}(f)N_{IJ}(f')] \end{aligned}$$

This expression reduces to the Eq. (4.3) in presence of only a single astrophysical source. Note that, in spite of being very large, this matrix is easy to handle because it is a diagonal matrix plus a low-rank correction. When no external information is available ($\Sigma^{-1} = 0$), the term in parenthesis has the only role of making the \mathbf{A} columns \mathbf{N}^{-1} -orthonormal, so that the spectrum of F on the space spanned by the foregrounds is zero (i.e., there is no information on any linear combination of the columns of \mathbf{A}).

Using F as the inverse variance, we can also compute $\int_0^\infty df \int_0^\infty df' F(f, f') z_{IJ}(f') z_{IJ}(f)$ to try to detect the presence of a signal in z_{IJ} that can not be explained as a statistical fluctuation of the noise or the astrophysical signal. Unfortunately, this can hardly be useful because this quantity is dominated by the immense number of low-SNR modes, which would likely shadow even fairly visible signals. We can select a family of modes $\{m_i(f)\}_{i=1, \dots, k}$ that we wish to use as a basis for the k -dimensional sub-space of admissible primordial backgrounds. These modes can be used to probe the SNR on them one-by-one with Eq. (4.4). It is probably more interesting, however, to project z_{IJ} on the entire subspace generated by the models of our choice and to compute the total SNR. Collecting the basis vector in the columns of the matrix \mathbf{M} , the minimum-variance fit to the data is

$$\hat{S}_p(f) = \mathbf{M} (\mathbf{M}^t \mathbf{F} \mathbf{M})^{-1} \mathbf{M}^t \mathbf{F} \mathbf{z}, \quad (\text{C.5})$$

and the SNR achieved is

$$\text{SNR}^2 = \mathbf{z}^t \mathbf{F} \mathbf{M} (\mathbf{M}^t \mathbf{F} \mathbf{M})^{-1} \mathbf{M}^t \mathbf{F} \mathbf{z}. \quad (\text{C.6})$$

These are the familiar expressions of the generalized least squared estimator, which arise when estimating the parameters of a linear model under a constraint of minimum variance. Note that, in general, the reconstructed amplitudes of the modes $\{m_i(f)\}_{i=1, \dots, k}$ —estimated using Eq. (C.5) without the leading \mathbf{M} —are correlated: Their covariance is $(\mathbf{M}^t \mathbf{F} \mathbf{M})^{-1}$.

We conclude this appendix with some computational remarks that can be relevant in this context when the number of sampled frequencies n is large. PCA computes the k eigenvectors $\{v_i(f)\}_{i=1, \dots, k}$ —collected in \mathbf{V} —and the corresponding eigenvalues $\{\lambda_i\}_{i=1, \dots, k}$. When the eigenvectors are employed for a template-free reconstruction, we get particularly simple expressions

$$\hat{S}_p(f) = \mathbf{V} \mathbf{V}^t \mathbf{z} \quad (\text{C.7})$$

and

$$\hat{S}_p(f) = \mathbf{z}^t \mathbf{V} \text{diag}(\lambda_1, \dots, \lambda_k) \mathbf{V}^t \mathbf{z}, \quad (\text{C.8})$$

which coincide with the expressions in Eq. (4.5) and (4.6). As we said in Section 4, we do not believe that PCA is interesting for the type of application discussed in this paper, but still we want to highlight that it is possible to do it when n is very large, even though an explicit calculation of the matrix and its decomposition would respectively require $O(n^2)$ storage locations and up to $O(n^3)$ operations. The most practical solution is to down-sample the frequencies until the brute-force calculation can be afforded, but the PCA can be performed without any down-sampling in order $O(k \times n)$ operations because the matrix (Fisher or covariance) is a diagonal matrix plus a low-rank correction. Such a simple structure allows to store the matrix with only few $O(n)$ locations—the spectrum of the noise and the astrophysical templates, whose number is of order unity—and to apply the matrix on a vector in $O(n)$ operations: It consists of few vector-vector and scalar-vector operations. We are not interested in the full set of eigenvectors and eigenvalues of the matrix, just in the k best constrained by our

experiment. The eigenvectors with the highest eigenvalues can be computed in $O(k)$ applications of the matrix—plus other $O(k)$ vector-vector products—using the Lanczos method. The overall $O(k \times n)$ scaling of this PCA poses no threat for any sensible value of n and k . Note, however, that this scaling is accurate only for $k \ll n$. When k is comparable with n , other $O(k^2)$ calculations internal to the Lanczos method start to be significant. The total scaling is still better than $O(n^3)$ but if n is small the prefactors can be significant. Even more important, the explicit solution to the eigenvalue problem internally uses matrix-matrix operations, compared to the vector-vector operations inside the application of our sparse Fisher matrix. The former run much faster than the latter on modern CPUs (and GPUs), so the time-to-completion of an iterative $O(k \times n)$ algorithm may result comparable (or even higher!) than a $O(n^3)$ algorithm for small values of n .

Lastly, we want to comment on the inversion of the covariance matrix. The analytical expression in Eq. (C.4) is reasonably simple to implement and handle (most important, it is diagonal with a low-rank correction, as the covariance matrix). Still one may prefer to work only with the covariance matrix instead of the Fisher matrix, in order to avoid the computation of $(\Sigma^{-1} + \mathbf{A}^t \mathbf{N}^{-1} \mathbf{A})^{-1}$. Eqs. (C.5) and (C.6) can be computed using only the ability of applying V on a vector by casting every application of F on a vector (or matrix) into an inverse problem with V as system matrix. If solved with the preconditioned conjugate gradient (PCG), the solution is achieved at most in a number of iterations equal to the number of astrophysical components, thus with few $O(n)$ operations. The reason is that the CG converges to the solution in a number of iterations lower than the number of distinct eigenvalues of the system matrix. Once preconditioned with the inverse of the first term in Eq. (C.2), the variance becomes the identity plus a low-rank correction and, therefore, the number of distinct eigenvalue is equal to this rank plus one.

References

- [1] Michele Maggiore. Stochastic backgrounds of gravitational waves. *ICTP Lect. Notes Ser.*, 3:397–414, 2001.
- [2] Nelson Christensen. Stochastic Gravitational Wave Backgrounds. *Rept. Prog. Phys.*, 82(1):016903, 2019.
- [3] Chiara Caprini and Daniel G. Figueroa. Cosmological Backgrounds of Gravitational Waves. *Class. Quant. Grav.*, 35(16):163001, 2018.
- [4] Tania Regimbau. The astrophysical gravitational wave stochastic background. *Res. Astron. Astrophys.*, 11:369–390, 2011.
- [5] B. P. Abbott et al. GW151226: Observation of Gravitational Waves from a 22-Solar-Mass Binary Black Hole Coalescence. *Phys. Rev. Lett.*, 116(24):241103, 2016.
- [6] B.P. Abbott et al. Observation of Gravitational Waves from a Binary Black Hole Merger. *Phys. Rev. Lett.*, 116(6):061102, 2016.
- [7] B.P. Abbott et al. Binary Black Hole Mergers in the first Advanced LIGO Observing Run. *Phys. Rev. X*, 6(4):041015, 2016. [Erratum: *Phys.Rev.X* 8, 039903 (2018)].
- [8] Benjamin P. Abbott et al. GW170104: Observation of a 50-Solar-Mass Binary Black Hole Coalescence at Redshift 0.2. *Phys. Rev. Lett.*, 118(22):221101, 2017. [Erratum: *Phys.Rev.Lett.* 121, 129901 (2018)].
- [9] B.. P.. Abbott et al. GW170608: Observation of a 19-solar-mass Binary Black Hole Coalescence. *Astrophys. J.*, 851(2):L35, 2017.

- [10] B.P. Abbott et al. GW170814: A Three-Detector Observation of Gravitational Waves from a Binary Black Hole Coalescence. *Phys. Rev. Lett.*, 119(14):141101, 2017.
- [11] B.P. Abbott et al. GW170817: Observation of Gravitational Waves from a Binary Neutron Star Inspiral. *Phys. Rev. Lett.*, 119(16):161101, 2017.
- [12] Alessandra Buonanno, Gunter Sigl, Georg G. Raffelt, Hans-Thomas Janka, and Ewald Muller. Stochastic gravitational wave background from cosmological supernovae. *Phys. Rev. D*, 72:084001, 2005.
- [13] Konstantin N. Yakunin et al. Gravitational Waves from Core Collapse Supernovae. *Class. Quant. Grav.*, 27:194005, 2010.
- [14] Valeria Ferrari, Sabino Matarrese, and Raffaella Schneider. Stochastic background of gravitational waves generated by a cosmological population of young, rapidly rotating neutron stars. *Mon. Not. Roy. Astron. Soc.*, 303:258, 1999.
- [15] Quan Cheng, Yun-Wei Yu, and Xiao-Ping Zheng. Stochastic gravitational wave background from magnetic deformation of newly born magnetars. *Mon. Not. Roy. Astron. Soc.*, 454(3):2299–2304, 2015.
- [16] Alexei A. Starobinsky. A New Type of Isotropic Cosmological Models Without Singularity. *Adv. Ser. Astrophys. Cosmol.*, 3:130–133, 1987.
- [17] Andrei D. Linde. A New Inflationary Universe Scenario: A Possible Solution of the Horizon, Flatness, Homogeneity, Isotropy and Primordial Monopole Problems. *Adv. Ser. Astrophys. Cosmol.*, 3:149–153, 1987.
- [18] Alan H. Guth. The Inflationary Universe: A Possible Solution to the Horizon and Flatness Problems. *Adv. Ser. Astrophys. Cosmol.*, 3:139–148, 1987.
- [19] Viatcheslav F. Mukhanov and G. V. Chibisov. Quantum Fluctuations and a Nonsingular Universe. *JETP Lett.*, 33:532–535, 1981.
- [20] M. Hazumi et al. LiteBIRD: A Satellite for the Studies of B-Mode Polarization and Inflation from Cosmic Background Radiation Detection. *J. Low Temp. Phys.*, 194(5-6):443–452, 2019.
- [21] Kevork Abazajian et al. CMB-S4 Science Case, Reference Design, and Project Plan. 7 2019.
- [22] T.W.B. Kibble. Topology of Cosmic Domains and Strings. *J. Phys. A*, 9:1387–1398, 1976.
- [23] Tanmay Vachaspati, Levon Pogosian, and Daniele Steer. Cosmic Strings. *Scholarpedia*, 10(2):31682, 2015.
- [24] Saswat Sarangi and S.H. Henry Tye. Cosmic string production towards the end of brane inflation. *Phys. Lett. B*, 536:185–192, 2002.
- [25] Nicholas T. Jones, Horace Stoica, and S.H. Henry Tye. The Production, spectrum and evolution of cosmic strings in brane inflation. *Phys. Lett. B*, 563:6–14, 2003.
- [26] Luca Pagano, Laura Salvati, and Alessandro Melchiorri. New constraints on primordial gravitational waves from Planck 2015. *Phys. Lett. B*, 760:823–825, 2016.
- [27] B.P. Abbott et al. Constraints on cosmic strings using data from the first Advanced LIGO observing run. *Phys. Rev. D*, 97(10):102002, 2018.
- [28] B.P. Abbott et al. GW150914: Implications for the stochastic gravitational wave background from binary black holes. *Phys. Rev. Lett.*, 116(13):131102, 2016.
- [29] Benjamin P. Abbott et al. GW170817: Implications for the Stochastic Gravitational-Wave Background from Compact Binary Coalescences. *Phys. Rev. Lett.*, 120(9):091101, 2018.
- [30] Zaven Arzoumanian et al. The NANOGrav 12.5-year Data Set: Search For An Isotropic Stochastic Gravitational-Wave Background. 9 2020.

- [31] R.w. Hellings and G.s. Downs. UPPER LIMITS ON THE ISOTROPIC GRAVITATIONAL RADIATION BACKGROUND FROM PULSAR TIMING ANALYSIS. *Astrophys. J. Lett.*, 265:L39–L42, 1983.
- [32] Zhen Pan and Huan Yang. Probing Primordial Stochastic Gravitational Wave Background with Multi-band Astrophysical Foreground Cleaning. *Class. Quant. Grav.*, 37(19):195020, 2020.
- [33] Raphael Flauger, Nikolaos Karnesis, Germano Nardini, Mauro Pieroni, Angelo Ricciardone, and Jesús Torrado. Improved reconstruction of a stochastic gravitational wave background with LISA. 9 2020.
- [34] Mauro Pieroni and Enrico Barausse. Foreground cleaning and template-free stochastic background extraction for LISA. *JCAP*, 07:021, 2020. [Erratum: JCAP 09, E01 (2020)].
- [35] Bruce Allen. The Stochastic gravity wave background: Sources and detection. In *Les Houches School of Physics: Astrophysical Sources of Gravitational Radiation*, pages 373–417, 4 1996.
- [36] Bruce Allen and Joseph D. Romano. Detecting a stochastic background of gravitational radiation: Signal processing strategies and sensitivities. *Phys. Rev. D*, 59:102001, 1999.
- [37] Michele Vallisneri and Chad R. Galley. Non-sky-averaged sensitivity curves for space-based gravitational-wave observatories. *Class. Quant. Grav.*, 29:124015, 2012.
- [38] Pau Amaro-Seoane, Heather Audley, Stanislav Babak, John Baker, Enrico Barausse, Peter Bender, Emanuele Berti, Pierre Binetruy, Michael Born, Daniele Bortoluzzi, Jordan Camp, Chiara Caprini, Vitor Cardoso, Monica Colpi, John Conklin, Neil Cornish, Curt Cutler, Karsten Danzmann, Rita Dolesi, Luigi Ferraioli, Valerio Ferroni, Ewan Fitzsimons, Jonathan Gair, Lluís Gesa Bote, Domenico Giardini, Ferran Gibert, Catia Grimani, Hubert Halloin, Gerhard Heinzl, Thomas Hertog, Martin Hewitson, Kelly Holley-Bockelmann, Daniel Hollington, Mauro Hueller, Henri Inchauspe, Philippe Jetzer, Nikos Karnesis, Christian Killow, Antoine Klein, Bill Klipstein, Natalia Korsakova, Shane L Larson, Jeffrey Livas, Ivan Lloro, Nary Man, Davor Mance, Joseph Martino, Ignacio Mateos, Kirk McKenzie, Sean T McWilliams, Cole Miller, Guido Mueller, Germano Nardini, Gijs Nelemans, Miquel Nofrarias, Antoine Petiteau, Paolo Pivato, Eric Plagnol, Ed Porter, Jens Reiche, David Robertson, Norna Robertson, Elena Rossi, Giuliana Russano, Bernard Schutz, Alberto Sesana, David Shoemaker, Jacob Slutsky, Carlos F. Sopuerta, Tim Sumner, Nicola Tamanini, Ira Thorpe, Michael Troebes, Michele Vallisneri, Alberto Vecchio, Daniele Vetrugno, Stefano Vitale, Marta Volonteri, Gudrun Wanner, Harry Ward, Peter Wass, William Weber, John Ziemer, and Peter Zweifel. Laser Interferometer Space Antenna. *arXiv e-prints*, page arXiv:1702.00786, February 2017.
- [39] Tristan L. Smith and Robert Caldwell. LISA for Cosmologists: Calculating the Signal-to-Noise Ratio for Stochastic and Deterministic Sources. *Phys. Rev. D*, 100(10):104055, 2019.
- [40] B.P. Abbott et al. Search for the isotropic stochastic background using data from Advanced LIGO’s second observing run. *Phys. Rev. D*, 100(6):061101, 2019.
- [41] Neil Cornish and Travis Robson. Galactic binary science with the new LISA design. *J. Phys. Conf. Ser.*, 840(1):012024, 2017.
- [42] Travis Robson, Neil J. Cornish, and Chang Liu. The construction and use of LISA sensitivity curves. *Class. Quant. Grav.*, 36(10):105011, 2019.
- [43] Paolo Campeti, Eiichiro Komatsu, Davide Poletti, and Carlo Baccigalupi. Measuring the spectrum of primordial gravitational waves with CMB, PTA and Laser Interferometers. 7 2020.
- [44] Matthew R. Adams and Neil J. Cornish. Detecting a Stochastic Gravitational Wave Background in the presence of a Galactic Foreground and Instrument Noise. *Phys. Rev. D*, 89(2):022001, 2014.